Precipitation of DNA by Polyamines: A Polyelectrolyte Behavior

E. Raspaud,* M. Olvera de la Cruz,# J.-L. Sikorav,§ and F. Livolant*

*Laboratoire de Physique des Solides, CNRS URA D0002, Université Paris Sud, 91405 Orsay Cedex, and #Service de Chimie Moléculaire and §Service de Biochimie et Génétique Moléculaire, CEA/Saclay, 91191 Gif-sur-Yvette, France

ABSTRACT Conditions of double-stranded DNA precipitation by the polyamines spermidine and spermine have been determined experimentally and compared to theoretical predictions. The influence of the concentrations of DNA and added monovalent salt, and of the DNA length has been investigated in a systematic manner. Three regimes of DNA concentrations are observed. We clarify the dependence of these regimes on the monovalent salt concentration and on the DNA length. Our observations make possible a rationalization of the experimental results reported in the literature. A comparison of the precipitation conditions of different kinds of polyelectrolytes suggests a general process. Our experimental data are compared to the "ion-bridging" model based on short-range electrostatic attractions. By starting from the spinodal equation, predicted by this model, and using the limiting form of Manning's fractions of condensed counterions, analytical expressions of the precipitation conditions have been found in the three regimes. Experimental and theoretical results are in good agreement.

INTRODUCTION

Ion condensation in the vicinity of DNA has been extensively studied and has a drastic influence on DNA conformation (for a review, see Bloomfield, 1997). Monovalent cation condensation is implicated, for example, in the stability and the flexibility of the double helix. Condensation of multivalent cations such as the polyamines spermine (4^+) or spermidine (3^+) stabilizes the DNA double helix (generally in its B-form) (Tabor, 1962; Gosule and Schellman, 1978) and leads to its precipitation (see, for instance, Razin and Rosansky, 1959). Equilibrium dialysis studies indicate that the interactions of these polyamines with DNA are predominantly electrostatic (Braunlin et al., 1982).

In the presence of polyamines or other multivalent cations, a monomolecular DNA collapse can occur in a highly dilute solution of long DNA chains (Widom and Baldwin, 1983), whereas multimolecular aggregation is generally observed in more concentrated solutions, regardless of the DNA length (Arscott et al., 1990). Porschke (1984) reports the existence of two processes occurring in dilute solutions of long DNA chains (λ, T4, and T7): a fast reaction, in the millisecond time range, associated with the intramolecular collapse, and a slower reaction, with typical time constants on the order of 100 s, assigned to a diffusion-controlled intermolecular process. For measurement times larger than these intermolecular times, it is not possible to experimentally separate collapse and aggregation processes; this was also observed by Widom and Baldwin (1983). The polyamine condensation in the vicinity of DNA can therefore lead to an individual collapse (only for long chains), to a multimolecular aggregation, and finally to a macroscopic precipitation of the DNA/polyamines system. Precipitation allows us to quantify ion condensation without the help of sophisticated local measurements.

The precipitation or the aggregation induced by tri- or tetravalent cation is not a consequence of the intrinsic structure and flexibility of DNA, but is a common feature of polyelectrolyte solutions. This is illustrated by two extreme examples. First, a recent study by light scattering and electron microscopy shows that several rodlike biopolymers (actin filaments, microtubules, etc.) form bundle-shaped aggregates in the presence of multivalent ions (Tang et al., 1996). In the second example, Delsanti et al. (1994) have built, by visual inspection and light scattering, a phase diagram for solutions of a synthetic polyelectrolyte, poly(styrene-sulfonate) (PSS). Contrary to the actin filament, this polymer is semiflexible, and in the studied concentration range, its persistence length is ~10 times smaller than that of DNA (Spiteri et al., 1996). Furthermore, an excess of multivalent cations leads to the redissolution of the aggregated chains for both PSS (Delsanti et al., 1994) and DNA (Pelta et al., 1996), and the phase diagrams of these two polyelectrolytes are roughly similar. These experimental results therefore clearly demonstrate that the common mechanism leading to precipitation or aggregation is qualitatively independent of the polymer flexibility. As a consequence, this common mechanism leads to collapsed chains, aggregates, or pellets, the internal structure of which may or may not be ordered, depending on the flexibility of the molecule. The common feature among all of these systems is, rather, their highly charged character, and this strongly suggests that electrostatic attractions must be taken into consideration to explain this mechanism.

In this work, we have used spermidine (3^+) and spermine (4^+) to precipitate DNA. The effects of monovalent salt

Received for publication 15 May 1997 and in final form 15 October 1997.

Address reprint requests to Dr. Eric Raspaud, Laboratoire de Physique des Solides, CNRS URA D0002, Université Paris Sud, 91405 Orsay Cedex, France. Tel.: 33-01-69-15-53-51; Fax: 33-01-69-15-60-86; E-mail: raspaud@lps.u-psud.fr.

Dr. Olvera de la Cruz's present address is Department of Materials Science and Engineering, Northwestern University, Evanston, IL 60208.

0006-3495/98/01/381/13 $2.00

concentration, DNA concentration, and molecular weight on the phase diagrams are investigated and compared with the results reported in the literature. A theoretical analysis of the experimental data is carried out using the "ion-bridging" model based on short-range electrostatic attractions developed by Olvera de la Cruz et al. (1995).

MATERIALS AND METHODS

Materials

Polydisperse (DNA) fragments (referred to here as "polydisperse fragments") were obtained as described by Sikorav et al. (1994) from a selective digestion of calf thymus chromatin (Strzelecka and Rill, 1987). The polydispersity of these fragments ranges from 50 to 10^3 bp. DNA fragments with a narrower polydispersity were obtained by fractionation of these polydisperse fragments. The lengths of these fragments (referred to here as "150-bp fragments") are between 130 and 600 bp, and 50% of them are 146 ± 7 bp (Sikorav et al., 1994). Bacteriophage λ DNA (5×10^4 bp) was purchased from GIBCO BRL, and T4 DNA (1.6×10^5 bp) was kindly provided by Dorothée Jary (CEA/Saclay). All DNA solutions were extensively dialyzed against a solution of TE buffer (10 mM Tris HCl, 1 mM EDTA, pH 7.6), or TE + 25 mM NaCl (pH 7.6) buffer, or 2 mM NaCl (pH 5.1). The ratio A_{260}/A_{280} of the absorbances of DNA solutions measured at 260 nm and 280 nm was between 1.8 and 1.85, indicating a protein-free preparation. NaCl, spermidine (3 HCl; Fluka), and spermine (4 HCl; Fluka) were also dissolved in the same buffers.

Methods

Various amounts of polyamines were added to the solutions of DNA and NaCl. Samples were then generally vortexed, incubated at room temperature for at least 15 min, and centrifuged at 11,000 × *g* for 7 min. The concentration of DNA in the supernatant was determined by the measurement of the absorbance at 260 nm. The precision of the relative absorbance is evaluated to be 0.005, which corresponds to a relative error of less than 8% in all cases. This relative error depends only on the DNA concentration and on its absorbance compared to the value 0.005. The concentration of polyamines required to induce a precipitation or a redissolution was then defined as the polyamine concentration at which the concentration of the supernatant and the initial DNA concentration differ by more than this relative error. We note that this definition differs from that used in previous studies, where these concentrations correspond to the midpoints of the transitions (half-point concentration between zero precipitation and the maximum value obtained in precipitation). Fig. 1 illustrates the determination of the spermidine concentrations of precipitation $C_{\text{precip.}}$ and of redissolution $C_{\text{redissol.}}$ in the case of λ DNA and 150-bp fragments. These solutions were diluted in TE + 25 mM NaCl at a monomer concentration equal to 9×10^{-3} mM and 0.9 mM, respectively (1 mg/ml of DNA corresponds to 3 mM phosphate). The precision of such determinations mainly depends on the number of experimental points. On average, the polyamine concentrations $C_{\text{precip.}}$ and $C_{\text{redissol.}}$ are determined within 15%. We have compared the results obtained in that way and those obtained by an increase of the incubation time and centrifugation force. For 150-bp fragments at a concentration equal to 0.9 mM in TE + 25 mM NaCl, we have performed measurements on samples vortexed, incubated for 1 week, and centrifuged at 30,600 × *g* for 10 min. Results are plotted on Fig. 1. The values of $C_{\text{precip.}}$ and $C_{\text{redissol.}}$ remain equal within 15%, but the percentage of DNA remaining in the supernatant depends on the procedure. This dependence on centrifugation conditions can be explained by a polydispersity of aggregate sizes.

In the case of high spermine concentrations, due to the absorbance of spermine at 260 nm, a standard curve has been established from measurements at 260 and 315 nm (Chayen and Denby, 1968). A linear relationship was found between the two measurements, which allows us to subtract the spermine absorbance and thus to measure the DNA absorbance of the samples.

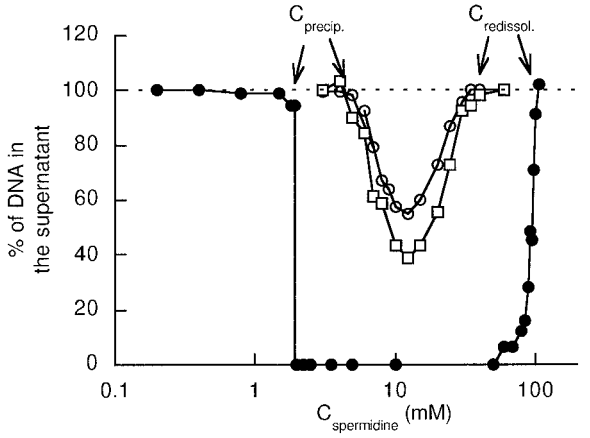

FIGURE 1 Variation of the DNA percentage present in the supernatant after centrifugation as a function of the spermidine concentration. The spermidine concentrations $C_{\text{precip.}}$ and $C_{\text{redissol.}}$ have been determined in the case of a TE + 25 mM NaCl buffer, for λ DNA at $C_{\text{DNA}} = 9 \times 10^{-3}$ mM (●), and for 150-bp fragments diluted at a concentration $C_{\text{DNA}} = 0.9$ mM centrifuged either at 11,000 × *g* (○) or at 30,600 × *g* (□).

In the case of solutions with a DNA concentration higher than 0.3 mM, supernatants were diluted in TE + 200 mM or 500 mM NaCl to a range measurable by optical density. This dilution allows us to determine the precipitation in an extended DNA concentration range (over 3 decades for 150-bp solutions). In the case of solutions with a DNA concentration higher than 9 mM, the $C_{\text{precip.}}$ and $C_{\text{redissol.}}$ concentrations were determined by visual inspection. Indeed, as they are sufficiently concentrated, these solutions are turbid or are even present as a pellet after vortexing in the concentration range between $C_{\text{precip.}}$ and $C_{\text{redissol.}}$.

RESULTS

Pelta et al. (1996) have found a precipitation of DNA at a polyamine concentration $C_{\text{precip.}}$ increasing smoothly with the DNA concentration C_{DNA}, and a redissolution in excess of spermine or spermidine at a concentration $C_{\text{redissol.}}$ nearly independent of C_{DNA}. The phase diagrams of the two systems DNA/polyamine and NaPSS/$La(Cl)_3$ or $Th(NO_3)_4$ (Delsanti et al., 1994) were found to be roughly similar. We present here a more detailed study and a comparison between DNA experiments.

DNA concentration and molecular weight effects

In Fig. 2, the spermine concentrations $C_{\text{precip.}}$ and $C_{\text{redissol.}}$ are plotted as a function of C_{DNA} over 4 decades for the 150-bp fragments and over less than 2 decades for λ DNA in TE buffer. The concentration $C_{\text{redissol.}}$ was measured only for the 150-bp fragments and found equal to 105 ± 10 mM over the whole DNA concentration range. For $C_{\text{precip.}}$, different variations corresponding to three regimes are observed. The three regimes are arrowed in Fig. 2. In the intermediate regime, in a C_{DNA} range between 0.1 and 10 mM, values obtained for the 150-bp fragments and those for λ DNA superimpose. In addition, the spermine concentra-

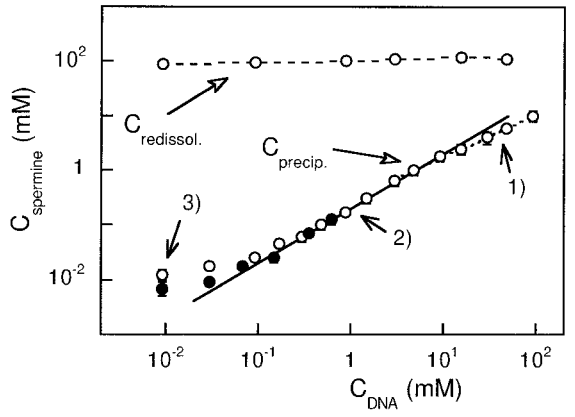

FIGURE 2 Spermine concentrations $C_{precip.}$ and $C_{redissol.}$ versus DNA concentration. Precipitation and redissolution conditions were obtained for solutions of 150-bp fragments (○) diluted in TE buffer and precipitation conditions for λ DNA solutions (●). The lines indicate three different fits: solid line, constant ratio $C_{precip.}/C_{DNA} = 0.20 \pm 0.02$; dashed line for the precipitation, a power law $C_{precip.} \approx C_{DNA}^{0.77 \pm 0.03}$; dashed line for the redissolution of the 150-bp fragments, a constant $C_{redissol.} = 105 \pm 10$ mM.

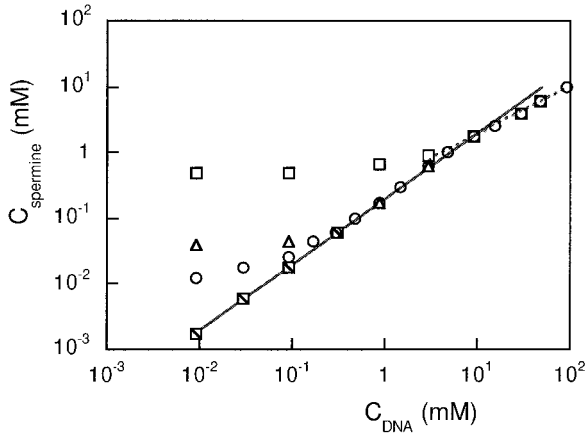

FIGURE 3 Effect of NaCl and TE concentrations on the precipitation conditions. The 150-bp fragments were precipitated by spermine at different NaCl and TE concentrations: ◱, 2 mM NaCl; ○, 10 mM TE; △, 10 mM TE + 10 mM NaCl; □, 10 mM TE + 75 mM NaCl. The lines are similar to those in Fig. 2.

tion $C_{precip.}$ increases linearly with C_{DNA}, and the ratio $C_{precip.}/C_{DNA}$ is found to be constant and equal to 0.20 ± 0.02. In the following, we will refer to this intermediate regime, where $C_{precip.}/C_{DNA}$ is proportional to 0.2, as the second regime or regime 2. The first regime (regime 1) is observed at high DNA concentrations (above 10 mM). Here the concentration $C_{precip.}$ deviates from the linearity, and the concentration $C_{precip.}$ follows a power law of exponent 0.77 ± 0.03 (indicated in Fig. 2 by the *dashed line*). As this regime is observed for just over one decade in C_{DNA}, this power law may be not effective. In this first regime, the ratio $C_{precip.}/C_{DNA}$ is lower than 0.2. The third regime (or regime 3) is observed at low DNA concentrations (below 0.1 mM in Fig. 2). Here the ratio $C_{precip.}/C_{DNA}$ is larger than 0.2; the concentration $C_{precip.}$ increases smoothly with C_{DNA} and depends on the molecular weight. In this last regime, the data may be fitted by a linear relationship $C_{precip.} = \alpha \times C_{DNA} + \beta$ (fit not shown; this linear relationship does not show up on the log-log plot of Fig. 2).

NaCl concentration effects in the three regimes

The influence of added NaCl on $C_{precip.}$ (measured for 150-bp fragments) is illustrated in Fig. 3. In addition to the increase in $C_{precip.}$ with the NaCl concentration, one may observe that NaCl does not affect $C_{precip.}$ in the same manner in the three regimes. In the third regime (for $C_{precip.}/C_{DNA} > 0.2$, at low C_{DNA} values), the spermine concentration $C_{precip.}$ becomes independent of C_{DNA}. The DNA concentration range of the third regime increases with increasing NaCl concentration. This effect has been reported in the literature. For example, Hoopes and McClure (1981) have found a spermine concentration $C_{precip.}$ independent of DNA concentration, over two decades, from 3 to 300 μM and at "moderate" salt buffer (10 mM Tris HCl, pH 8, 0.1 mM KCl, 10 mM $MgCl_2$). Widom and Baldwin (1983) have observed a similar behavior in the case of highly dilute solutions of λ and 1/2λ DNA chains collapsed by cobalthexamine; they found a cobalthexamine concentration required for the collapse ($C_{collapse}$) that was independent of the DNA concentration but dependent on the molecular weight.

In the first and second regimes (with $C_{precip.}/C_{DNA} < 0.2$ and $C_{precip.}/C_{DNA} \cong 0.2$, respectively), the addition of NaCl has a different effect. The spermine concentration $C_{precip.}$ is independent of the NaCl concentration, and the DNA concentration range of the second regime shrinks with the addition of NaCl. The independence of $C_{precip.}$ of the monovalent salt concentration is noteworthy. It means that in the first and second regimes, the spermine concentration required for precipitation or aggregation does not depend on the kind of added salt, its concentration, or the DNA molecular weight.

In the third regime, another effect on $C_{precip.}$ is observed at high C_{NaCl}. At $C_{TE+NaCl} \geq 110$ mM, there is no more detectable precipitation of the 150-bp fragments at the lowest DNA concentration (9×10^{-3} mM). This C_{DNA} threshold, below which no precipitation occurs, increases with the monovalent salt concentration; at $C_{TE+NaCl} \geq 210$ mM, for instance, DNA fragments at a concentration equal to 9×10^{-2} mM do not precipitate. This threshold may be considered as the junction of the precipitation and the redissolution curves, enclosing the phase separation region.

Conditions of precipitation and redissolution in the third regime

The concentration $C_{precip.}$ measured in the third regime is plotted in Fig. 4 (for spermine) and in Fig. 5 (for spermidine) as a function of the monovalent salt concentration $C_{TE+NaCl}$. For 150-bp and polydisperse fragments, the measurements have been performed at various DNA concentra-

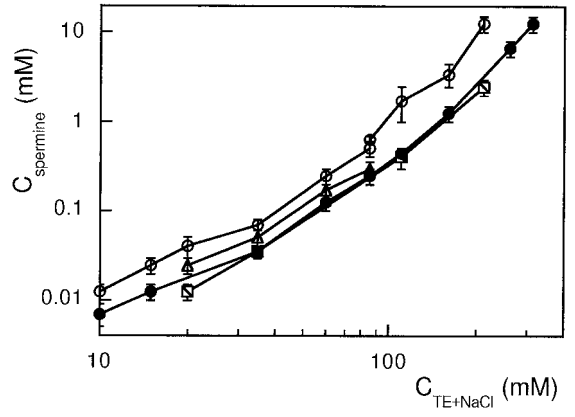

FIGURE 4 Variation of spermine concentration $C_{precip.}$ as a function of the added monovalent salt concentration in the first regime. The different symbols correspond to different molecular weights: ○, 150-bp fragments; △, polydisperse fragments; ●, λ DNA; ◫, T4 DNA.

tions, and for λ and T4 DNA, only at 9×10^{-3} mM. The concentration $C_{precip.}$ of multivalent cations increases with $C_{TE+NaCl}$. These results are in agreement with those obtained by Widom and Baldwin (1983) for cobalthexamine. These authors reported a slope of 0.6 in a log-log plot of $Co^{3+}(NH_3)_6$ versus Na^+ concentrations. However, this power law holds only for a limited range of Na^+ concentration (between 0.5 and 2 mM). At higher concentrations, the slope is reported to increase, leading to a convex curve similar to the curves obtained here. These results contrast with those of Subirana and Vives (1981), which were obtained for the same NaCl range. Subirana and Vives reported the existence of a slope of 2.6 in a log-log plot of spermine versus Na^+ concentrations. Even if we consider that this discrepancy is due to the mixture of monovalent salts (10 mM TE + various amounts of NaCl), we do not find a power law of exponent equal to 2.6 in the range where the Tris-HCl concentration (10 mM) is negligible compared

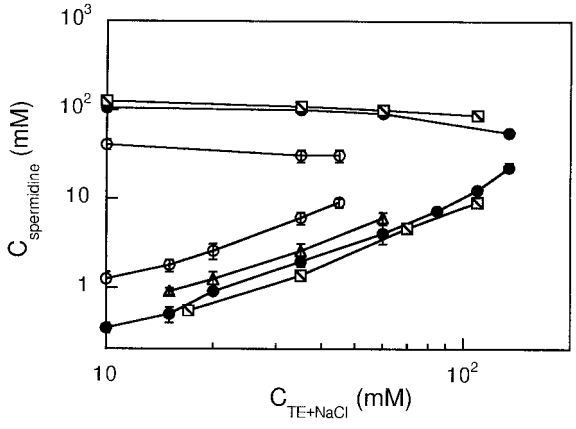

FIGURE 5 Variation in the spermidine concentrations, which makes it possible to precipitate and to redissolve DNA in the first regime, as a function of the monovalent salt concentration for different molecular weights. The symbols are the same as in Fig. 4.

to C_{NaCl}. The only difference between the two experiments is the presence of Tris-HCl, which in our case maintains the pH of the solution at 7.6.

In Figs. 4 and 5, a similar increase in $C_{precip.}$ with $C_{TE+NaCl}$ is observed independently of molecular weight. It must be recalled that because the fractionated and unfractionated fragments are polydisperse, the concentrations $C_{precip.}$ and $C_{redissol.}$ are mainly sensitive to the longest chains (equal to 600 bp and 10^3 bp, respectively). In Figs. 4 and 5, one notes that the fractionation has an important effect on the $C_{precip.}$ value. In return, the $C_{precip.}$ values for polydisperse fragments ($\leq 10^3$ bp) are close to those measured for λ and T4 DNA (within 30%). One may thus consider that the molecular weight effect on $C_{precip.}$ is important for short DNAs but is attenuated when DNA is sufficiently long. This effect was previously obtained by Marquet et al. (1987) for DNA lengths between 750 and 6000 bp.

In Fig. 5, the spermidine concentration of redissolution $C_{redissol.}$ is also plotted as a function of $C_{TE+NaCl}$ for 150-bp fragments, λ, and T4 DNA. Unlike $C_{precip.}$, the concentration $C_{redissol.}$ decreases smoothly when $C_{TE+NaCl}$ increases, and increases with molecular weight. In other words, the coexistence range that constitutes the phase diagram is broadened when the DNA molecular weight increases. This feature is also observed for NaPSS (Delsanti et al., 1994).

Minimum of the DNA supernatant concentrations

As shown in Fig. 1, the DNA concentration in the supernatant may present a minimum $C_{min.\ supernatant}$ detectable by absorbance measurement. As the value of this minimum concentration depends on the centrifugation conditions (cf. Methods), we have been interested in its variation rather than in its absolute value. Using identical experimental conditions (same incubation times and centrifugation conditions), we have measured $C_{min.\ supernatant}$ as a function of the initial DNA concentration $C_{initial}$ for different ionic conditions. Results are plotted in Fig. 6 for the 150-bp and the polydisperse fragments. Surprisingly, Fig. 6 shows an identical increase in $C_{min.\ supernatant}$ with $C_{initial}$, whatever the type of polyamine and whatever the monovalent salt concentration. This increase is fitted by a power law with an average exponent equal to 0.68 ± 0.02 (close to 2/3). This power law holds over 2 decades of $C_{initial}$. For comparison, a dashed line corresponding to the first bissectrice (of exponent 1) and to the limit of precipitation is also drawn in Fig. 6.

For a given monovalent salt concentration, the concentrations of polyamines required for the maximum precipitation of DNA chains are curiously found to be independent of the initial DNA concentration (in the studied range) and of the centrifugation procedure (cf. Fig. 1). Furthermore, in the case of spermidine, the values of this concentration are found to increase linearly with the monovalent salt concentration (data not shown); these values, measured for the 150-bp fragments, the unfractioned fragments, and the λ

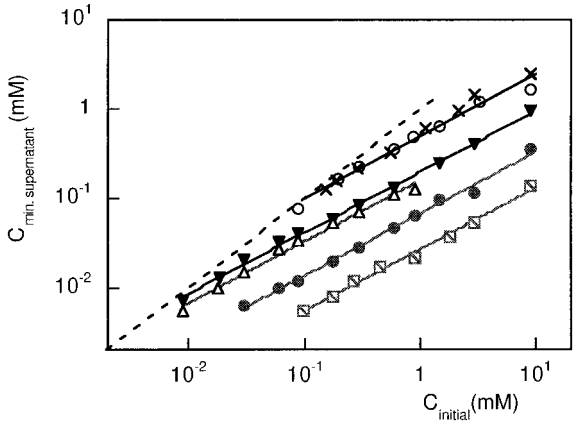

FIGURE 6 Minimum concentration of DNA in the supernatant for samples centrifuged at 11,000 × *g* as a function of the initial DNA concentration. Symbols: For spermidine, 150-bp fragments diluted in TE + 25 mM NaCl (○) and in TE + 10 mM NaCl (▼); polydisperse fragments in TE + 25 mM NaCl (△). For spermine, 150-bp fragments diluted in TE + 200 mM NaCl (×), in TE + 150 mM NaCl (●), and in TE + 50 mM NaCl (□). In all cases, the data are well fitted by a power law with an exponent 0.68 ± 0.02, indicated by straight lines. The dashed line represents the first bissectrice ($C_{min.\ supernatant} = C_{initial}$), indicating the precipitation limit.

DNA, are aligned on the same straight line and are localized in the middle of the phase separation lines $C_{precip.}$ and $C_{redissol.}$ (data not shown).

DISCUSSION

Polyelectrolyte aggregation or precipitation has long been and is still extensively studied (see, for instance, Bungenberg de Jong, 1949, for a historical perspective, and Barrat and Joanny, 1996, for a recent review). Because chains carrying the same charges are expected a priori to repel each other, the attractive force responsible for this self-assembly must be due to the presence of counterions. In the case of monovalent counterions, the existence of an attractive force between two rodlike polyelectrolytes mediated by an overlap of condensed counterion sheaths has been proposed by Ray and Manning (1994). Experimentally, aggregation in standard conditions is generally not observed, except in the experiments of Wissenburg et al. (1995), performed on DNA fragments in concentrated solutions. In the case of multivalent counterions, several theories have been developed to explain the chain aggregation or precipitation. The common feature of these theories is the prediction of a dominant local attraction (either via an electrostatic process or via a chemical process known as complexation; Wittmer et al., 1995). For instance, the electrostatic interaction resulting from the fluctuations of condensed counterion concentrations in the sheath of two polyelectrolytes is expected to be attractive at short distances on the order of the Bjerrum length (defined in the following section) (Oosawa, 1971; Barrat and Joanny, 1996). An "ion-bridging" model has been developped by Olvera de la Cruz et al. (1995) to account for the existence of an electrostatic attraction. This model relies on the existence of a random alternation of negative and positive charges along the polyelectrolyte. In this model, the different fractions of condensed ions are determined using the Poisson-Boltzmann equations. This model has been used to study poly(styrene-sulfonate) solutions. More recently, Rouzina and Bloomfield (1996) have developed another model, where the surface of the counterion sheath is composed of a periodic alternation of positive and negative charges. A spatial correlation of condensed counterions belonging to two different polyelectrolytes is observed, resulting in an electrostatic attraction. In this article, we will consider a modified form of the "ion-bridging" model, where the different fractions of condensed ions are determined by Manning's theory (Manning, 1978).

An "ion-bridging" model

This modified "ion-bridging" model describes the phase diagrams of highly charged polyelectrolyte chains. It can explain some of the features of the DNA phase diagram shown in Fig. 2. The ion condensation notion, in the case of linear chains, involves the classical structural parameter $\xi = l_B/b$, where l_B and b are, respectively, the Bjerrum length and the distance between adjacent charges (for double-stranded DNA, $\xi = 4.2$). The Bjerrum length l_B corresponds to the characteristic distance for which the electrostatic interaction potential between two unit charges (e) in solution counterbalances their thermal energy (kT). According to the model of ion condensation introduced by Manning (1978), highly charged polyelectrolyte chains (HCPCs) are chains with a distance b such that $\xi > 1/|z_i z_m|$, where z_i and z_m are the valences of the ions in the solution and of the charged units of the chains, respectively. In HCPCs, the ions condense along the chains, and the "ion-bridging" model shows that the condensation of multivalent ions can lead to the precipitation of the chains. The model presented here incorporates the condensation of the ions along the HCPC chains, and the resulting interactions in the equation that determines the limit of instability of the homogeneously mixed state (the spinodal line). The phase separation of this homogeneously mixed state corresponds to its decomposition in two macroscopic phases, one rich in polymer and the other rich in solvent.

We recall that the phase separation of a polymeric solution is described by two curves, the coexistence curve and the spinodal curve. The first one is obtained by equating the chemical potentials of all the components in the two phases; it is computed from the first derivative of the free energy and allows us to determine the composition of the two phases. The spinodal line itself is obtained by setting to zero $\partial^2 F/\partial\varphi^2$, the second derivative of the free energy F with respect to the polymer concentration φ ($\varphi = \rho_m a^3$, where ρ_m is the polymer density and a is the size of the monomer). The spinodal curve determines when the homogeneous one-phase system is first unstable, i.e., when an infinitesimal concentration fluctuation of infinite extension decreases the

free energy of the system, resulting in its decomposition. The spinodal line, however, gives only the limit of instability of the one-phase region, and does not correspond to the coexistence line, which occurs before the system is unstable. Starting from a one-phase region and progressively decreasing the solvent quality, the system crosses the coexistence curve first, passes through the metastable region, and finally crosses the spinodal line, to reach the spinodal region (cf., for instance, de Gennes, 1979). When a system is in the spinodal region, a fluctuation in the composition of infinitesimal magnitude will initiate the decomposition (spinodal decomposition). In contrast, when the system is between the coexistence and the spinodal lines, it is metastable, and the decomposition occurs only when a sufficiently large composition fluctuation of a size bigger than a critical nucleus occurs (i.e., there is an energy barrier to the decomposition process).

In many cases, it is difficult to determine precisely whether the decomposition limit observed experimentally corresponds to the coexistence or spinodal curves, or if it is located within the metastable or spinodal regions. For instance, in the case of neutral polymeric solutions, Grosberg and Kuznetsov (1992) have determined quantitatively the theoretical phase diagram of polystyrene solutions and have compared this diagram to the experimental diagrams. It appears that, depending on the experimental groups and on the degree of polymerization of the chains, the decomposition limits observed can correspond to any of the four possibilities mentioned above (i.e., superimposition on the spinodal or coexistence curves, or localization within the metastable or spinodal regions).

In our system, the Flory-Huggins free energy of mixing reads

$$F/kT = (\varphi/N)\ln\varphi + (1-\varphi)\ln(1-\varphi) + \chi\varphi(1-\varphi) \quad (1)$$

where χ is the Flory interaction parameter, which describes the solvent quality. In Eq. 1, the two first terms come from the translational entropy of the chains and of the solvent molecules, respectively, and the last term from the energy term describing the interactions. In the limit of dilute polymer concentrations, the spinodal line corresponding to the second derivative, $\partial^2 F/\partial\varphi^2 = 0$, is given by

$$1/(N\rho_m) + v = 0 \quad (2a)$$

and as explained above, the system is unstable (within the spinodal region) when

$$1/(N\rho_m) + v < 0 \quad (2b)$$

where v is the effective monomer-monomer interaction or second virial coefficient. In neutral systems, v is equal to v_0, with

$$v_0 = a^3(1-2\chi) \quad (3)$$

In fact, $v = v_0$ corresponds to the integral d^3r of $[1 - \exp(-U(r)/kT)]$, where $U(r)$ is the potential at a distance r from the monomer. The integral from $r = 0$ to $r = a$, the monomer size, with a hard-core infinite potential, gives the first term in Eq. 3, which is the volume of the monomers a^3. The second term, $-2\chi a^3$, comes from the integral of the effective van der Waals interactions per thermal energy, χ, for which $[1 - \exp(-U(r)/kT)] \approx U(r)/kT$. Therefore, according to Eqs. 2a and 3, in neutral systems, the decomposition is due to a competition of the translational entropy terms of the chains and solvent molecules, $1/(N\rho_m)$ and a^3, respectively, with the net interaction χ.

In charged systems there are electrostatic contributions to the second virial coefficient, $v = v_0 + v^{ele}$. We shall construct v^{ele}, assuming that when the polymers in the solution are highly charged, the strong electrostatic attraction between the monomers and the ions in the solution gives rise to the condensation of a fraction of the ions along the polymer. Throughout this section we denote by subscript i the initial monovalent ions present in the solution, before the high-valence salt ions are added, and by subscript + the high-valence salt added. The charge per monomer, $z_m = -1$, is modified in the neighborhood of the condensed ions (we assume here that b, the distance between charges, is equal to the monomer size a). In the presence of monovalent ions ($z_i = 1$ at a density ρ_i) and other high-valence ions ($z_+ > 1$ at a density ρ_+), a fraction f_i and a fraction f_+ of the monomers have a condensed ion of valence z_i and z_+, respectively. There are three types of monomers: A, B, and C. Monomer A carries a monovalent condensed ion; monomer B has no condensed counterions; and monomer C carries a condensed ion of valence z_+. Therefore, the effective valences of the A, B, and C monomers are $z_A = z_i - 1 = 0$, $z_B = -1$, and $z_C = z_+ - 1$, respectively, and their concentrations are $\rho_A = f_i\rho_m$, $\rho_B = (1 - f_+ - f_i)\rho_m$, and $\rho_C = f_+\rho_m$. The virial v^{ele} must include all of the electrostactic interactions resulting from this condensation. For example, the electrostatic virial coefficient between the C and B particles is given by

$$v_{CB}^{ele} = \int d^3r\{1 - \exp(-U_{CB}(r)/kT)\} \quad (4)$$

where

$$U_{CB}(r)/kT = l_B z_C z_B \exp(-\kappa r)/r \quad (5)$$

is the screened Coulombic potential and κ is the screening constant of the ions that contribute to screening of the interactions between the C and B monomers in the solution. Equation 4 is integrated, expanding the exponential. The expansion up to first order in $U_{CB}(r)$ gives the Debye-Huckel approximation,

$$v_{CB}^{DH} = 4\pi l_B z_C z_B/\kappa^2 \quad (6)$$

Summing all of the contributions (v_{BB} and v_{CC}), weighted by their probability, one obtains

$$v^{DH} = 4\pi l_B z_{eff}^2/\kappa^2 \quad (7)$$

where z_{eff} is the average (effective) monomer valence after the ions condensed,

$$z_{\text{eff}} = (z_+ f_+ + z_i f_i - 1) \tag{8}$$

which can also be expressed as

$$v^{\text{DH}} = \kappa_{\text{em}}^2/(\kappa^2 \rho_m)$$

where κ_{em} is the "screening" from the monomers,

$$\kappa_{\text{em}}^2 = 4\pi l_B z_{\text{eff}}^2 \rho_m \tag{9}$$

At the Debye-Huckel level of approximation, the electrostatic contribution to the left-hand side of Eq. 2a is always positive. The effectively charged chains repel each other, helping to stabilize the solution. The corrections to Debye-Huckel due to electrostatic attractions ($U_{\text{CB}}(r) < 0$) are large at short distances, because in that case $\exp(-U_{\text{CB}}(r)/kT)$ is very large and a linearization (expansion until first order in $U_{\text{CB}}(r)/kT$) is not appropriate. Integrating the second order term in the expansion gives

$$v_{\text{CB}}^{(2)} = -\pi(l_B z_C z_B)^2/\kappa \tag{10}$$

This term must therefore be included when there are electrostatic attractions, such as between the C and B monomers. The contribution must also be weighted by the fraction of such binary contacts, $2f_+(1 - f_+ - f_i)$. Because B and C have opposite charges, they strongly attract each other. These attractions are responsible for the precipitation of the HCPC in the solution when ions of high valence condense on the polyelectrolyte.

Adding the electrostatic virial coefficient,

$$v^{\text{ele}} = v^{\text{DH}} - 2f_+(1 - f_+ - f_i)\pi(l_B z_C z_B)^2/\kappa \tag{11}$$

to the spinodal equation, we obtain the limit of instability of a charged polymer solution:

$$1/N + \rho_m v_0 + \kappa_{\text{em}}^2/\kappa^2 - \rho_m 2f_+(1 - f_+ - f_i)\pi(l_B z_C z_B)^2/\kappa = 0 \tag{12}$$

Equation 12 shows that even when the solvent (water) is a good solvent ($v_0 > 0$), one can have segregation in effectively charged chains ($z_{\text{eff}} < 0$) because of the short-range attractions betwen the C and B monomers. From now on we assume that initially, before the high-valence salt is added, only the monovalent counterions that make the polymer solution electrically neutral are present. Therefore, by electroneutrality ($\rho_i z + \rho_m z_m = 0$), the initial monovalent concentration ρ_i is equal to ρ_m. In the approximation that only the free ions contribute to the screening, κ^2 is equal to

$$\kappa^2 = 4\pi l_B(z_i^2 \rho_i^f + z_-^2 \rho_- + z_+^2 + \rho_+^f) \tag{13}$$

where ρ_i^f and ρ_+^f are the concentrations of free monovalent counterions and free high-valence salt ions, respectively, and ρ_- is the concentration of the counterions of the high-valence salt added, $\rho_- = (-z_+/z_-)\rho_+ = z_+\rho_+$. (In Olvera de la Cruz et al., 1995, it was shown that the condensed counterions contribute to the screening but are weighted by a reduced factor, because they do not move all along the system, but only along the polymer. Here this effect is neglected.)

In this model it is necessary to find f_i and f_+ to evaluate the spinodal. The values of f_i and f_+ in Eq. 12 must be computed, in principle, from the free energy, equating the chemical potentials of the condensed and free ions when the system decomposes. These fractions, in principle, will be a function of the chain conformation. There is, however, a universal region where the solution of Eq. 12 is indeed independent of the details of the system, such as chain conformation. This region corresponds to a polymer in the hypothetical case, where all of the high-valence ions added to the solution are condensed along the polymer ($f_+ = \rho_+/\rho_m$), and where there are no condensed monovalent ions ($f_i = 0$). This region is quite workable when the added salt consists of high-valence ions, because they are most attracted to the strongly charged polyelectrolyte. The initially condensed counterions (before the high-valence salt is added) are therefore replaced by high-valence condensed ions. In such circumstances, the effective charge of the polymer is

$$z_{\text{eff}} = (z_+ f_+ + z_i f_i - 1) = z_+\rho_+/\rho_m - 1 \tag{14a}$$

and

$$\kappa^2 = 4\pi l_B(\rho_m + z_+\rho_+) \tag{14b}$$

Because $z_{\text{eff}} < 1$, the transition must be at a salt concentration ρ_+ less than ρ_m/z_+, giving a value of ρ_+ at the spinodal, denoted by ρ_+^*. Substituting Eq. 14 in Eq. 12, we obtain the spinodal line,

$$1/N + \rho_m v_0 + (z_+\rho_+^*/\rho_m - 1)^2/(1 + z_+\rho_+^*/\rho_m) - \rho_+^*(1 - \rho_+^*/\rho_m)(z_+ - 1)^2\{\pi l_B^3/(\rho_m[1 + z_+\rho_+^*/\rho_m])\}^{1/2} = 0 \tag{15a}$$

where ρ_+^* is the value of the salt added at which the system is unstable. In this region the first two terms are negligible, and the above equation can be rewritten as

$$(x - 1)^2/(1 + x)^{1/2} - Ax(1 - x/z_+) = 0 \tag{15b}$$

where $x = z_+\rho_+^*/\rho_m$, and $A = (z_+ - 1)^2(\pi l_B^3 \rho_m)^{1/2}/z_+$. Because $\rho_m \ll 1$, $x = 1 - \epsilon$, with $\epsilon \approx [2^{1/2}A(1 - 1/z_+)]^{1/2} - A(1 - 2/z_+)/2^{1/2}$, the model predicts an instability independent of both N and the conformation at

$$\rho_+^* = (\rho_m/z_+)\{1 - (z_+ - 1)(2\pi l_B^3 \rho_m)^{1/4}[(1 - 1/z_+)/z_+]^{1/2} + (z_+ - 1)^2(\pi l_B^3 \rho_m)^{1/2}(1 - 2/z_+)/(2^{1/2} z_+)\} \tag{16}$$

For example, for $\rho_m = C_{\text{DNA}} = 10^{-1}$ mM $= 6.023 \times 10^{-8}$ particles/Å^3 in Fig. 2 (setting $z_+ = 4$ and $l_B = 7$ Å in water), we obtain ρ_+^* ($= C_{\text{precip.}}$) $\approx 0.217\rho_m$, whereas for $\rho_m = 1$ mM, $\rho_+^* \approx 0.194\rho_m$. The approximation gets worse as ρ_m increases.

Actually, this region is predicted by Manning's model to exist in the presence of high-valence salt. This model is

applicable to an infinitely long charged polymer with a charge density $\xi > 1$. In the case of only monovalent counterions and high-valence salt ions, the model in its limiting form predicts three regions, which we denote a, b, and c, depending on the value of $r_+ = z_+\rho_+/\rho_m$. They are related to the three experimental regimes in the manner discussed below.

The three theoretical regions a, b, and c are shown in Fig. 7 *a*, where we have plotted the fraction of initial condensed monovalent counterions $\alpha_i = \rho_i^{cond}/\rho_i$ and the fraction of condensed multivalent salt ions $\alpha_+ = \rho_+^{cond}/\rho_+$ versus r_+. In the absence of multivalent salt, $r_+ = 0$, Manning's theory predicts the saturated fraction $\alpha_i = 1 - 1/\xi$, which for DNA is equal to 0.76 ($\xi = 4.2$). The added multivalent cations replace first the initial condensed monovalent counterions, and if we assume that a multivalent cation replaces z_+ initial monovalent counterions, the value of α_i then decreases linearly as r_+ increases, up to a ratio of r_+^{1C}. At this ratio ($r_+^{1C} = 1 - 1/\xi$), all initial monovalent counterions are free (the fraction α_i becomes equal to 0), and only the multivalent ions are condensed. This delimits the region a of Manning, which for DNA and $z_+ = 4$ corresponds to $\rho_+ < 0.19\rho_m$. The value of α_+ in this region is equal to 1; that is, all of the added multivalent ions are condensed. The value of α_+ remains equal to 1 throughout the next region (region b), given by $r_+^{1C} < r_+ < r_+^{2C}$, where $r_+^{2C} = 1 - 1/(z_+\xi)$ corresponds to the saturation limit of multivalent cation condensation. For DNA and $z_+ = 4$, region b is given by $0.19\rho_m < \rho_+ < 0.235\rho_m$. For $r_+ > r_+^{2C}$, α_+ decreases and should tend toward zero when the amount of added multivalent salt is very high. Compared to the DNA concentration, the multivalent salt is in excess, and the concentration of free multivalent cation increases linearly with its total concentration. This region is denoted by region c. In Fig. 7 *b* we have plotted the three regions, a, b, and c, of the Manning model in a log-log curve of ρ_m ($= C_{DNA}$) versus ρ_+ ($= C_{spermine}$) and superimposed an experimental curve ρ_+^* ($= C_{precip.}$) taken from Fig. 2. This figure shows that the region where ρ_+^* is nearly ρ_m independent (the most dilute polymer regime experimentally studied) corresponds to Manning's region c. Furthermore, the nearly linear relation $\rho_+^* = 0.2\rho_m$ is confined to Manning's region b, and the more concentrated polymer regime corresponds to region a of Manning. The three experimental regimes 1, 2, and 3 are therefore located in the theoretical regions a, b, and c, respectively. Below we solve the spinodal line, using Manning's theory in its limiting form in the three regions. The distribution of the initial monovalent and added multivalent cations is illustrated in Fig. 8 for the three regions.

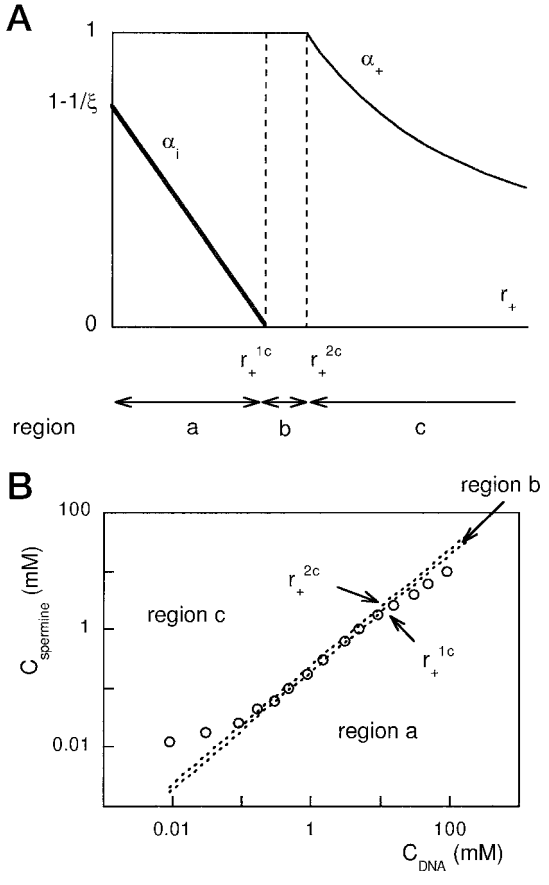

FIGURE 7 (*a*) Three regions of condensation of initial (monovalent) counterions and added high-valency (multivalent) ions. The fractions of initial condensed counterions (*thick line*) and the fraction of condensed multivalent salt ions (*thin line*), $\alpha_i = \rho_i^{cond}/\rho_i$ and $\alpha_+ = \rho_+^{cond}/\rho_+$, respectively, are plotted as a function of $r_+ = z_+\,\rho_+/\rho_m$. (*b*) Localization of the three regions a, b, and c in the diagram ($\rho_m = C_{DNA}$, $\rho_+ = C_{spermine}$) and comparison with the experimental data presented in Fig. 2 (○ corresponds to the 150-bp fragments diluted in TE buffer). The two parallel dotted lines enclosing region b correspond to the two equations $\rho_+ = \rho_m(1 - 1/\xi)/z_+$ and $\rho_+ = \rho_m(1 - 1/(z_+\xi))/z_+$, given by the constant ratios $r_+^{1C} = 1 - 1/\xi$ and $r_+^{2C} = 1 - 1/(z_+\xi)$, respectively.

Region a

In region a, both initial monovalent and multivalent cations are condensed, and there are only monovalent cations free in solution. Manning's theory gives the fractions of monomers having a condensed ions, $f_i = (1 - 1/\xi) - z_+\rho_+/\rho_m$ and $f_+ = \rho_+/\rho_m$. Therefore, the spinodal line is given by

$$1/N + \rho_m v_0 + (1/\xi)^2/(\rho_m(1/\xi + 2z_+\rho_+^*/\rho_m) - (1/\xi + (z_+ - 1)$$
$$\cdot\,\rho_+^*/\rho_m)(z_+ - 1)^2\{\pi l_B^3/(\rho_m[1/\xi + 2z_+\rho_+^*/\rho_m])\}^{1/2} = 0 \quad (17)$$

Clearly, the first two terms are negligible in this region. For ρ_m concentrations such that r_+ is close to r_+^{1C} but still with $1/\xi < (z_+ - 1)\rho_+^*/\rho_m$, Eq. 17 gives

$$\rho_+^* = \rho_m^{4/5}/(\xi^4 2z_+(z_+ - 1)^6\pi l_B^3)^{1/5} \quad (18)$$

When the concentration of polymer increases (ρ_+^* decreases), we find the region $(z_+ - 1)\rho_+^*/\rho_m < 1/\xi < 2z_+\rho_+^*/\rho_m$, for which Eq. 17 gives

$$\rho_+^* = \rho_m^{2/3}/(\xi^2 2z_+(z_+ - 1)^4\pi l_B^3)^{1/3} \quad (19)$$

For DNA with salt valence ions $z_+ = 4$, when $\rho_m = 10$ mM, Eq. 18 gives $\rho_+^* = 2$ mM, whereas for $\rho_m = 100$ mM, it

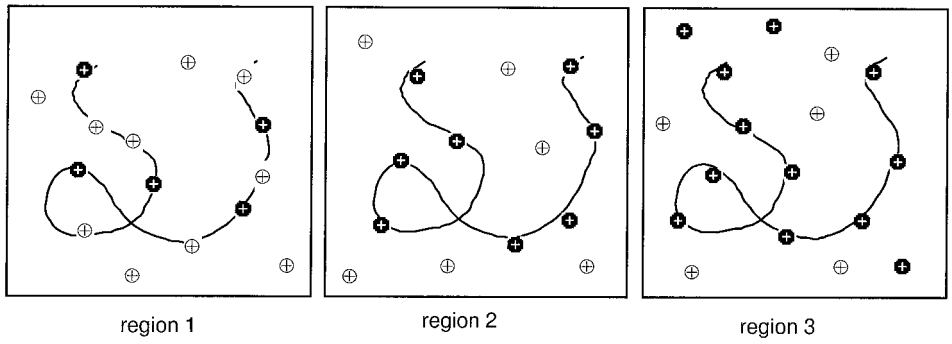

FIGURE 8 Distribution of the initial monovalent (○) and added multivalent (●) cations in the three theoretical regions.

gives $\rho_+^* = 12.8$ mM, very close to the value given by Eq. 19, $\rho_+^* = 12$ mM. This is not unexpected, because this value corresponds to a crossover for the applicability of Eqs. 18 and 19. These equations are in close agreement with the experimental results reported in Fig. 2. Indeed, experimentally, in regime 1, one obtains a variation $C_{\text{precip.}} \approx C_{\text{DNA}}^{0.77\pm0.03}$ for $C_{\text{spermine}}/C_{\text{DNA}} \geq 0.11$ that is close to the theoretical prediction given by Eq. 18, $\rho_+^* \approx \rho_{\text{m}}^{4/5}$ for $\rho_+/\rho_{\text{m}} > 0.08$.

For larger polymer concentrations, such that $2z_+\rho_+^*/\rho_{\text{m}} < 1/\xi$ (a region not studied experimentally), Eq. 17 gives

$$\rho_+^* = \rho_{\text{m}}^{1/2}/(\xi(z_+ - 1)^4\pi l_{\text{B}}^3)^{1/2} \tag{20}$$

Region b

In region b, the initial monovalent counterions are completely free and the added multivalent cations are all condensed. Manning's theory gives, then, the values reported in Eq. 14, and the spinodal line is therefore given by Eq. 16. Inside this region, there is no constraint of saturated condensation (given by the limiting formulae of Manning), and the spinodal line is independent of the charge density ξ. Moreover, as in Eq. 15a, the term associated with the translational entropy of the chains is negligible, which means that the instability limit is predicted to be independent of the molecular weight, in agreement with the results presented in Fig. 2, in the second regime.

Finally, one may also note that in regime 2, the experimental data on the precipitation lead to a constant ratio $C_{\text{spermine}}/C_{\text{DNA}} = 0.20 \pm 0.02$, which suggests that there exists a constant fraction f_+ of DNA phosphates carrying a condensed spermine, regardless of the DNA concentration. However, this idea is not consistent with the theoretical model, which predicts a weak variation of the fraction $f_+ = \rho_+/\rho_{\text{m}}$ (from $(1 - 1/\xi)/z_+ = 0.19$ to $(1 - 1/(z_+\xi))/z_+ = 0.235$. This variation, however, is experimentally undetectable.

Region c

In region c, the initial monovalent cations are all free, and there are both free and condensed multivalent cations. Because Manning's theory gives the constant saturation fraction $f_+ = (1 - 1/(z_+\xi))/z_+ = \alpha_+\rho_+/\rho_{\text{m}}$, the spinodal equation is given by

$$1/N + \rho_{\text{m}}v_0 + \rho_{\text{m}}/(z_+\xi)^2/(\rho_+z_+(1 + z_+)(1 - \epsilon) - B\rho_{\text{m}}/(\rho_+z_+(1 + z_+)(1 - \epsilon))^{1/2} = 0 \tag{21a}$$

where

$$\epsilon = \rho_{\text{m}}(z_+ - 1/\xi - 1)/(z_+\rho_+(1 + z_+)) \tag{21b}$$

and

$$B = (\pi l_{\text{B}}^3)^{1/2}(1 - 1/(z_+\xi))(1 - 1/z_+ + 1/(z_+^2\xi))(z_+ - 1)^2/z_+ \tag{21c}$$

Notice that Eq. 21 has two solutions: ρ_+^* and ρ_+^{**}. For $\rho_+^* < \rho_+ < \rho_+^{**}$, the left-hand side of Eq. 21a is negative, showing the two-phase region of instability. This explains the redissolution as the salt concentration increases above ρ_+^{**}, which is given by

$$\rho_+^{**} = B^2/((1/(N\rho_{\text{m}}) + v_0)^2z_+(1 + z_+)) \tag{22}$$

suggesting that the redissolution is strongly dependent on v_0. The value of v_0 may change as salt is added, because the van der Waals interactions are affected when the ions are condensed along the polymer.

Because the precipitation in region c is at very low polymer concentrations, the first two terms in Eq. 21a cannot be neglected. In the limit of infinitely long chains and for $v_0 = 0$, we obtain

$$\rho_+^*z_+(z_+ + 1) = 1/((z_+\xi)^2B)^2 + \rho_{\text{m}}(z_+ - 1 + 1/\xi) \tag{23}$$

which, when ρ_{m} goes to zero, ρ_+^* is a constant equal to 3.7×10^{-4} mM. Therefore, for DNA and $z_+ = 4$, Eq. 21 gives a linear relationship,

$$\rho_+^*(\text{mM}) = 0.14\rho_{\text{m}} + 3.7 \times 10^{-4} \tag{24}$$

For finite N, the corrections are

$$\rho_+^* = \delta[1 + \delta z_+(z_+ + 1)/(\rho_{\text{m}}N)^2(1 + 2\delta z_+(z_+ + 1)/(\rho_{\text{m}}N)^2)] \tag{25}$$

where

$$\delta = [\gamma^2 + B^2(z_+ - 1 + 1/\xi)\rho_{\text{m}}]/\{(B^2 - 2\gamma/(N\rho_{\text{m}}))z_+(z_+ + 1)\}$$

and

$$\gamma = 1/(z_+\xi)^2 - (z_+ - 1 + 1/\xi)/N$$

It works for $\rho_+^* z_+(z_+ + 1)/(\rho_m N)^2 \ll 1$. For a typical value ($\rho_m = 10^{-2}$ mM), this approximation breaks down for $N < 1000$. Actually, at $N = 914$, independently of ρ_m, γ is negative and other approximations are more appropriate.

In this region (c) or in the experimental regime (3), the prediction of the precipitation and redissolution conditions is delicate, because no term can be neglected in Eq. 21. This is due to the presence of free ions, which screen the electrostatic interactions. In particular, the screening due to an excess of free multivalent ions prevents the phase separation and induces a redissolution of the DNA chains.

In this context of strong screening, one can understand why the two concentrations $C_{\text{precip.}}$ and $C_{\text{redissol.}}$ depend on the chemical nature of the added cations, as shown by Pelta et al. (1996) for spermidine and cobalthexamine (both 3^+ cations). This dependence is likely to originate from the nonelectrostatic interaction terms (via v_0). One can also understand why the experimental concentrations $C_{\text{precip.}}$ and $C_{\text{redissol.}}$ are sensitive to the molecular weight for small DNA chains: we suggest that this dependence comes from the translational entropy of the chains. However, the theoretical predictions (Eqs. 22 and 25) do not quantitatively account for the experimental dependence on the molecular length of the two concentrations.

Indeed, according to Eq. 22, the redissolution concentration ρ_+^{**} depends not solely on N, but also on the product $\rho_m \times N$. This variation is not observed experimentally, because the concentration $C_{\text{redissol.}}$ is found to depend on the molecular length but not on the DNA concentration.

According to Eq. 25, the precipitation concentration ρ_+^* follows two kinds of variation with the monomer concentration ρ_m: starting from very low ρ_m values, the concentration ρ_+^* sharply decreases and then increases slightly when ρ_m increases. The smaller the length of the DNA chains, the smaller the period of increasing concentration, and it may even disappear. This prediction was not observed experimentally, but perhaps we should use smaller fragments.

In contrast, one expects that the junction between precipitation and redissolution lines occurs in the period of decreasing concentration. This was observed experimentally, although the curve has not been established. In the case of large N, the variations predicted by Eqs. 22 and 24 are also in good agreement with the experimental observations: the concentration of redissolution is independent of the DNA concentration, and the concentration of precipitation follows a linear relationship as a function of the DNA concentration, $C_{\text{precip.}} = \alpha \times C_{\text{DNA}} + \beta$.

To summarize the comparison between theoretical and experimental results, the analytical equations predicted in the three regions (Eqs. 16, 18, and 24) have been compared in Fig. 9 to the experimental data obtained for 150-bp fragments diluted in TE buffer and in 2 mM NaCl. Data

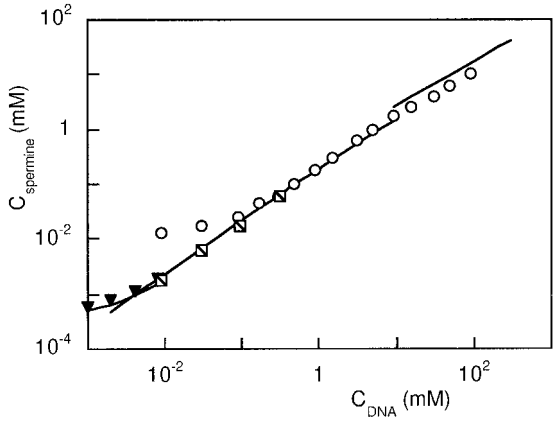

FIGURE 9 Comparison between experimental data and theoretical predictions in the three regions (Eqs. 24, 16, and 18 in regions c, b, and a, respectively). ○, □, 150-bp fragments diluted in TE pH 7.6 buffer and in 2 mM NaCl pH 5.1, respectively. ▼, Data deduced from figure 2 of Porschke (1984) (λ DNA solution in 4 mM NaCl, 4 mM sodium cacodylate, pH 6.4).

determined by Porschke (1984) on λ DNA are also included in Fig. 9. The agreement is quite surprising. We conclude that Manning's model in its limiting form, together with the simple spinodal equation, is in excellent agreement with our results. To find the coexistence curve (i.e., the composition of the two phases), the free energy must be computed; this will be done elsewhere.

Further theoretical work is also required to take into account the effect of monovalent salt (NaCl), which is added experimentally. Because the concentration of added monovalent salt ρ_{NaCl} is lower than or of the order of the multivalent ion concentration ρ_+, the corrections are not large, and the theoretical results in regions a and b do not change. This is not the case for region c, which is very sensitive to the addition of monovalent salt. For $\rho_{\text{NaCl}} \gg \rho_+$, i.e., in the experimental conditions, the theoretical situation becomes more complex and will be discussed elsewhere. Actually, it can be considered that the addition of NaCl implies that a fraction of these new Na^+ ions will condense, most probably changing the different fractions f and, consequently, the diagram shown in Fig. 7 *a*. As mentioned by Olvera de la Cruz et al. (1995), the addition of NaCl decreases the number of condensed multivalent counterions, and NaCl participates in the electrostatic screening via κ, resulting in a decrease in the effect of the "ion-bridging" attraction. We will come back to this point of discussion later.

Comparison with the results reported in the literature on DNA solutions

Most of the experiments reported in the literature have been performed in the third regime, and the reported ratio $C_{\text{precip.}}/C_{\text{DNA}}$ of the data is always close to or larger than 0.2. Moreover, the different characteristics of collapse, aggregation, and/or precipitation conditions determined by the

different authors are in good agreement with our observations in the third regime:

1. The concentration $C_{\text{precip.}}$ is sensitive to the addition of the monovalent salt and to the molecular weight of small DNA chains (cf., for instance, Osland and Kleppe, 1977, who report a molecular weight dependence on $C_{\text{precip.}}$ for short $d(A\text{-}T)_n$ fragments).

2. The concentration $C_{\text{precip.}}$ follows a linear relationship with the DNA concentration of the type $C_{\text{multivalent cation}} = \alpha \times C_{\text{DNA}} + \beta$.

The fact that some ratio $C_{\text{precip.}}/C_{\text{DNA}}$ of the data given in the literature remains close to but higher than 0.2 may be explained by the difference in definition of the concentration $C_{\text{precip.}}$, corresponding in the present work to the onset of precipitation, and in previous works to the midpoint of the transition as explained above. The midpoint concentration must be used carefully, and only for transitions where initial and final states are well defined. We think that this is the case for the coil-globule transition, but not for the coils-aggregates transition, because aggregates do not display a stable, well-defined size with time (cf., for instance, the electron micrographs reported by Ma et al., 1995). The DNA aggregates cannot be compared, for example, to surfactant or copolymer micelles, because there is no thermodynamic reason to explain a well-defined size of the aggregates. These aggregates remain in solution or precipitate according to their size, and the aggregation process may be compared to a macroscopic phase separation or to a demixing process. On that account, the ratio of $C_{\text{spermine}}/C_{\text{DNA}}$ (with C_{spermine} corresponding to the onset of the transition and therefore to the solubility line) reported in the literature in low monovalent salt buffer may be in good agreement with the value 0.20 ± 0.02. For instance, the ratio obtained from Porschke's experiments performed at 8 μM with λ DNA is equal to 0.185 ± 0.015 (Porschke, 1984), and that from Marquet's experiments, performed at 75 μM with 6000-bp DNA, is between 0.19 and 0.24 (Marquet et al., 1985).

As already noted, most of the experimental results reported in the literature correspond to the third experimental regime, with $\rho_{\text{NaCl}} \gg \rho_{+} \gg \rho_{\text{m}}$. These are the conditions that have been treated by Manning (1978), and indeed, using Manning's theory, one finds that both mono- and multivalent cations are condensed when collapse (or precipitation) occurs (cf., for instance, Wilson and Bloomfield, 1979).

The hypotheses that have been used here to give a theoretical description of region c are different ($\rho_{\text{NaCl}} = 0$). As a result, in our description, one finds only multivalent condensed cations. This makes the connection between Manning's conditions and ours difficult. We have considered adding a fraction of condensed Na^+ cations in region c to approach Manning's conditions. The difficulty is then to find the limit of the applicability of such an approach. In regions a and b, the precipitation conditions are found to be insensitive to the concentration of added monovalent salt. This implies that such an approach is of no benefit for the understanding of regions a and b. The applicability of this approach seems to be restricted, therefore, to a portion of region c, the boundaries of which are difficult to define.

Comparison with other polyelectrolytes

Similar experiments have been performed on other polyelectrolytes and other multivalent cations. The different studied polyelectrolytes may be viewed either as flexible chains (single-stranded DNA and poly(styrene-sulfonate)) or as rodlike chains (actin filaments and microtubules). Their highly charged nature constitutes their unique common characteristic. In all cases, the observations reported in the literature are found to be surprisingly similar to those made for double-stranded DNA solutions, regardless of the flexibility. We have reported here some of the observed characteristic features:

1. In the case of single-stranded DNA, Chaperon and Sikorav (personal communication) have observed a redissolution in excess of cobalthexamine (3^+) and of spermine (4^+), and an absence of aggregation at low C_{DNA} and at high C_{NaCl}. Experiments performed on macrocyclic bisacridine 1 (4^+) by Slama-Schwok et al. (1997) show a concentration $C_{\text{aggregation}}$ independent of C_{DNA} and a strong dependence of $C_{\text{aggregation}}$ on the molecular weight of the short DNA chains. All of these observations are characteristic of experimental regime 3.

2. In the case of poly(styrene-sulfonate), a constant ratio $C_{\text{precip.}}/C_{\text{PSS}}$ has been found by Narh and Keller (1993) with $AlCl_3$ (3^+) and by Delsanti et al. (1994) with $LaCl_3$ (3^+) and $Th(NO_3)_4$ (4^+). Delsanti et al. have also shown chain redissolution and reported phase diagrams on their systems. These diagrams are similar to the diagram plotted in Fig. 2, and the solubility lines follow the same variation: a constant ratio $C_{\text{precip.}}/C_{\text{PSS}}$ and a concentration $C_{\text{redissol.}}$ nearly independent of the monomer concentration. Moreover, the constant ratio is found to be independent of the molecular weight (between 4×10^3 and 1.6×10^6 g/mol). In the presence of 50 mM NaCl, the authors have also observed the characteristics of our regimes 2 and 3. In particular, in regime 2, the ratio $C_{\text{precip.}}/C_{\text{PSS}}$ is constant and independent of the presence of added monovalent salt. This observation indicates that in theoretical region b and in the presence of added NaCl, one cannot include a fraction of Na^+ condensed ions, as discussed above.

3. In the case of actin filaments and microtubules, Tang et al. (1996) have reported bundle formation by cobalthexamine (3^+) and polylysine (18^+). They also found the different characteristics of regime 3, for instance, an independence of $C_{\text{aggregation}}$ with the molecular weight for the longest actin filaments, and a concentration of microtubules following a linear relationship of type $\alpha \times C + \beta$.

It should be mentioned that another parameter, different from the flexibility, changes in all of the systems reported here. As the polystyrene chain that constitutes the poly(styrene-sulfonate) skeleton is well known to be highly hydro-

phobic, one may think a priori that its precipitation results from a neutralization of the sulfonate charged group and then from the local repulsion between the skeleton and the water. But, as noted by Olvera de la Cruz et al. (1995), this argument is mistaken, because all of the polyelectrolytes reviewed here are certainly not constituted by a hydrophobic skeleton. Thus the charge neutralization by multivalent cations is not sufficient to explain the precipitation, and one has to involve another process, such as an electrostatic attraction. Although monovalent cations alone can induce aggregation theoretically (Ray and Manning, 1994) and experimentally (Wissenburg et al., 1995), we think that the short-range electrostatic attractions in the presence of multivalent ions are responsible for the precipitation, as in the model of Rouzina and Bloomfield (1996).

In conclusion, we found experimentally three regimes of DNA concentration that have been explained theoretically by the ion-bridging model, restricted to the case where no monovalent ions are added:

1. At high DNA concentration (first regime), we found experimentally that the conditions of precipitation do not depend on the added monovalent ion concentration; they vary as $C_{\text{multivalent ions}} \approx C_{\text{DNA}}^{0.77 \pm 0.03}$. This variation is in good agreement with the theoretical predictions. Moreover, we predict that the precipitation conditions depend only on the charge density ξ of the chains. In these conditions, multivalent cations are all condensed on the chains, whereas monovalent ions are partly condensed and partly free in solution.

2. At low DNA concentration (third regime), the experimental conditions of precipitation depend on all parameters (molecular length and added monovalent salt concentration); they vary as $C_{\text{multivalent ions}} = \alpha \times C_{\text{DNA}} + \beta$. The dependences on these parameters and on the charge density are expected theoretically. In the restricted case of no added monovalent salts, precipitation occurs when only multivalent cations are condensed, with both monovalent and multivalent cations free in solution.

3. In the medium range of DNA concentration (second regime), we show experimentally that there is no dependence on the polymer length or added monovalent ion concentration; conditions of precipitation vary as $C_{\text{spermine}}/C_{\text{DNA}} = 0.20 \pm 0.02$, in good agreement with theoretical predictions. We also predict that there is no dependence on flexibility or the charge density of the polymer, or on the shape of the particle. It is thus a universal regime that, in principle, could also be observed with colloidal polyelectrolyte suspensions. The only condition for the existence of this universal regime is a workable state in which all of the multivalent cations are condensed, with no condensed monovalent ions.

We thank Juan Pelta and Amélie Leforestier for many fruitful discussions, and Dorothée Jary for providing us with T4 DNA. We sincerely thank the anonymous referees and the editor, V. A. Bloomfield, for their help in improving the manuscript.

This work was supported by a grant from the Ministère de l'Enseignement Supérieur et de la Recherche (ACC-SV5).

REFERENCES

Arscott, P. G., A.-Z. Li, and V. A. Bloomfield. 1990. Condensation of DNA by trivalent cations. 1. Effects of DNA length and topology on the size and shape of condensed particles. *Biopolymers.* 29:619–630.

Barrat, J.-L., and J.-F. Joanny. 1996. Theory of polyelectrolyte solutions. *In* Advances in Chemical Physics, Vol. XCIV. I. Prigogine and S. A. Rice, editors. John Wiley and Sons, New York. 16–20.

Bloomfield, V. A. 1997. Polymer and polyelectrolyte behavior of DNA. Proceedings of the International Interdisciplinary Conference "Structure and Function of DNA: A Physical Approach" (Mont Sainte-Odile, France, Sept.–Oct., 1996). *In* Nucleic Acids: Structures, Properties, and Functions. V. A. Bloomfield, D. M. Crothers, and I. Tinoco, Jr., editors. University Science Books, Mill Valley, CA. In press.

Braunlin, W. H., T. J. Strick, and M. T. Record. 1982. Equilibrium dialysis studies of polyamine binding to DNA. *Biopolymers.* 21:1301–1314.

Bungenberg de Jong, H. G. 1949. Complex colloid systems. *In* Colloid Science, Vol. 2. H. R. Kruyt, editor. Elsevier Science Publishing Co., New York. 335–432.

Chayen, J., and E. F. Denby. 1968. Biophysical Technique As Applied to Cell Biology. K. Mellanby, editor. Methuen and Co., London. 85–86.

de Gennes, P.-G. 1979. Scaling Concepts in Polymer Physics. Cornell University Press, Ithaca, NY. 98–127.

Delsanti, M., J. P. Dalbiez, O. Spalla, L. Belloni, and M. Drifford. 1994. Phase diagram of polyelectrolytes solutions in presence of multivalent salts. *In* Macro-Ion Characterization from Dilute Solutions to Complex Fluids. K. S. Schmitz, editor. *ACS Symp. Ser.* 548:381–392.

Gosule, L. C., and J. A. Schellman. 1978. DNA condensation with polyamines I. Spectroscopic studies. *J. Mol. Biol.* 121:311–326.

Grosberg, A. Y., and D. V. Kuznetsov. 1992. Phase separation of polymer solutions and interactions of globules. *J. Phys. II France.* 2:1327–1339.

Hoopes, B. C., and W. R. McClure. 1981. Studies of the selectivity of DNA precipitation by spermine. *Nucleic Acids Res.* 9:5493–5505.

Ma, C., L. Sun, and V. A. Bloomfield. 1995. Condensation of plasmids enhanced by Z-DNA conformation of $d(CG)_n$ inserts. *Biochemistry.* 34:3521–3528.

Manning, G. S. 1978. The molecular theory of polyelectrolyte solutions with applications to the electrostatic properties of polynucleotides. *Q. Rev. Biophys.* 11:179–246.

Marquet, R., C. Houssier, and E. Fredericq. 1985. An electro-optical study of the mechanisms of DNA condensation induced by spermine. *Biochim. Biophys. Acta.* 825:365–374.

Marquet, R., A. Wyart, and C. Houssier. 1987. Influence of DNA length on spermine-induced condensation. Importance of the bending and stiffening of DNA. *Biochim. Biophys. Acta.* 909:165–172.

Narh, K. A., and A. Keller. 1993. Precipitation effects in polyelectrolytes on addition of salts. *J. Polym. Sci. B Polym. Phys.* 31:231–234.

Olvera de la Cruz, M., L. Belloni, M. Delsanti, J. P. Dalbiez, O. Spalla, and M. Drifford. 1995. Precipitation of highly charged polyelectrolyte solutions in the presence of multivalent salts. *J. Chem. Phys.* 103: 5781–5791.

Oosawa, F. 1971. Polyelectrolytes. Marcel Dekker, New York. 123–126.

Osland, A., and K. Kleppe. 1977. Polyamine induced aggregation of DNA. *Nucleic Acids Res.* 4:685–695.

Pelta, J., F. Livolant, and J.-L. Sikorav. 1996. DNA aggregation induced by polyamines and cobalthexamine. *J. Biol. Chem.* 271:5656–5662.

Porschke, D. 1984. Dynamics of DNA condensation. *Biochemistry.* 23: 4821–4828.

Ray, J., and G. S. Manning. 1994. An attractive force between two rodlike polyions mediated by the sharing of condensed counterions. *Langmuir.* 10:2450–2461.

Razin, S., and R. Rosansky. 1959. Mechanism of the antibacterial action of spermine. *Arch. Biochem. Biophys.* 81:36–54.

Rouzina, I., and V. A. Bloomfield. 1996. Macroion attraction due to electrostatic correlation between screening counterions. 1. Mobile surface-adsorbed ions and diffuse ion cloud. *J. Phys. Chem.* 100: 9977–9989.

Sikorav, J.-L., J. Pelta, and F. Livolant. 1994. A liquid crystalline phase in spermidine-condensed DNA. *Biophys. J.* 67:1387–1392.

Slama-Schwok, A., F. Peronnet, E. Hantz-Brachet, E. Taillandier, M. P. Teulade-Fichou, J.-P. Vigneron, M. Best-Belpomme, and J.-M. Lehn. 1997. A macrocyclic bis-acridine shifts the equilibrium from duplexes toward DNA hairpins. *Nucleic Acids Res.* 25:2574–2581.

Spiteri, M. N., F. Boué, A. Lapp, and J.-P. Cotton. 1996. Persistence length for a PSSNa polyion in semi-dilute solution as a function of the ionic strength. *Phys. Rev. Lett.* 77:5218–5220.

Strzelecka, T. E., and R. L. Rill. 1987. Solid-state ^{31}P NMR studies of DNA liquid crystalline phases. The isotropic to cholesteric transition. *J. Am. Chem. Soc.* 109:4513–4518.

Subirana, J. A., and J. L. Vives. 1981. The precipitation of DNA by spermine. *Biopolymers.* 20:2281–2283.

Tabor, H. 1962. The protective effect of spermine and other polyamines against heat denaturation of deoxyribonucleic acid. *Biochemistry.* 1:496–501.

Tang, J. X., S. Wong, P. T. Tran, and P. A. Janmey. 1996. Counterion induced bundle formation of rodlike polyelectrolytes. *Ber. Bunsenges. Phys. Chem.* 100:796–806.

Widom, J., and R. L. Baldwin. 1983. Monomolecular condensation of λ-DNA induced by cobalthexamine. *Biopolymers.* 22:1595–1620.

Wilson, R. W., and V. A. Bloomfield. 1979. Counterion-induced condensation of desoxyribonucleic acid. A light-scattering study. *Biochemistry.* 18:2192–2196.

Wissenburg, P., T. Odijk, P. Cirkel, and M. Mandel. 1995. Multimolecular aggregation of mononucleosomal DNA in concentrated isotropic solutions. *Macromolecules.* 28:2315–2328.

Wittmer, J., A. Johner, and J.-F. Joanny. 1995. Precipitation of polyelectrolytes in the presence of multivalent salts. *J. Phys. II France.* 5:635–654.